JOURNAL OF SPACECRAFT AND ROCKETS
Vol. 45, No. 2, March–April 2008

Transition Experiments on Blunt Bodies with Distributed Roughness in Hypersonic Free Flight

D. C. Reda* and M. C. Wilder†
NASA Ames Research Center, Moffett Field, California 94035-1000
and
D. W. Bogdanoff‡ and D. K. Prabhu‡
ELORET Corporation, Sunnyvale, California 94086

DOI: 10.2514/1.30288

Models of hemispherical and blunt large-angle conical geometries were flown in the NASA Ames hypersonic ballistic range to investigate the influence of distributed surface roughness on transition to turbulence. Transition-zone fronts were defined from optically measured global surface temperature distributions. Measurements of preconditioned surface roughness, surface temperature, average transition-front location, and freestream environment were combined with real-gas Navier–Stokes calculations of model flowfields, including laminar boundary-layer development in these flowfields, to transform all data into dimensionless parameters used to correlate transition onset/location on rough blunt bodies in hypersonic flow. A combination of present and previously published results led to the formulation of a transition correlation applicable over all three regimes potentially encountered by an ablating blunt-body heat shield undergoing atmospheric entry: the smooth-wall asymptote, the critical-roughness Reynolds number regime, and the large-roughness/low-Reynolds-number asymptote.

Nomenclature

B'	=	$\dot{m}/\rho_e u_e C_m$
C_m	=	Stanton number for mass transfer
D_{base}	=	model base diameter
h	=	measured in-plane surface roughness height
$\bar{h}$	=	average in-plane surface roughness height
$\bar{k}$	=	average roughness height
$\dot{m}$	=	mass flux from surface
P_∞	=	freestream static pressure
R_N	=	nosetip radius
Re	=	Reynolds number
s	=	arc length from the stagnation point
T	=	temperature
u	=	velocity
V_∞	=	model velocity at the measurement station
X	=	$[\rho_k u_k \bar{k}/\rho_e u_e \theta]$
Y_{tr}	=	$[\rho_e u_e \theta/\mu_w]_{\text{tr}}$
θ	=	laminar boundary-layer momentum thickness
θ_c	=	frustum cone half-angle
μ	=	fluid viscosity
ρ	=	fluid density

Subscripts

e	=	evaluated at the boundary-layer edge
k	=	evaluated at the roughness height
smooth	=	smooth wall
stag	=	stagnation point
tr	=	transition
w	=	evaluated at the wall conditions
∞	=	freestream

Presented as Paper 0306 at the 45th AIAA Aerospace Sciences Meeting and Exhibit, Reno, NV, 8–11 January 2007; received 5 February 2007; revision received 5 October 2007; accepted for publication 10 October 2007.

*Senior Staff Scientist, Space Technology Division, Mail Stop 229-3. Fellow AIAA.
†Aerospace Engineer, Reacting Flow Environments Branch, Mail Stop 230-2. Associate Fellow AIAA.
‡Senior Research Scientist. Associate Fellow AIAA.

I. Introduction

MODELING of roughness-dominated transition is an important design issue for many ablating thermal protection systems (TPS). Ablating TPS for single-use planetary-entry and Earth-return missions first experience recession under high-altitude low-Reynolds-number conditions. Such laminar-flow ablation causes the formation of a distributed surface microroughness pattern characteristic of the TPS material composition and fabrication process. Once formed, these distributed surface roughness elements create disturbances within the laminar boundary layer flowing over the surface. As altitude decreases, Reynolds number increases, and flowfield conditions capable of amplifying these roughness-induced perturbations are eventually achieved; that is, transition onset occurs. Boundary-layer transition to turbulence results in more severe heat transfer rates. Ablating TPS thus can potentially encounter failure mechanisms associated with exceeding bond-line temperature limits, burn-through, or thermostructural breakup.

The objective of this paper was to extend the earlier work of the lead author [1–5] to encompass relevant published results and newly acquired data concerning transition on blunt bodies with distributed roughness in quiet, compressible-flow, environments. The resultant transition correlation covers all three regimes potentially encountered by any blunt/ablating TPS: 1) the smooth-wall limit, wherein laminar-ablation-induced roughness elements are extremely small compared with viscous laminar boundary-layer length scales (e.g., the momentum thickness); 2) the roughness-dominated regime, wherein the laminar-ablation-induced roughness elements are comparable in scale with the laminar boundary-layer momentum thickness; and 3) the large-roughness/low-Reynolds-number asymptote, wherein the laminar-ablation-induced roughness elements have become large compared with viscous length scales, and hence further increases in roughness-element height either have no additional influence on breakdown to turbulence or the unit Reynolds number has become low enough that roughness-induced disturbances, no matter how large, fail to amplify and subsequently die out.

II. Existing Transition Correlation for the Roughness-Dominated Regime

Figure 1, taken from the review paper of Reda [5], shows a plot of preablated graphite blunt-body transition data measured in hypersonic-ballistic-range experiments. The disturbance parameter is composed of a dimensionless momentum flux ratio $[\rho_k u_k/\rho_e u_e]$ multiplied by a dimensionless roughness-element height $\bar{k}/\theta$. The dependent variable is a transition Reynolds number based on density and velocity at the boundary-layer edge and viscosity calculated at the wall (roughness element) temperature. The characteristic viscous length scale is taken to be the laminar boundary-layer momentum thickness θ.

Calculations of real-gas flowfields and laminar boundary-layer development within these flowfields were made here and throughout this work using the data-parallel line-relaxation (DPLR) code of [6]. DPLR is a high-fidelity aerothermal analysis tool developed in-house at NASA Ames Research Center. It incorporates the best available physical models for thermochemical nonequilibrium flows. Based on a finite volume implementation of a modified Steger–Warming flux-splitting method with Gauss–Seidel line relaxation, DPLR is a parallel multiblock code. Nominal third-order spatial accuracy for inviscid fluxes is obtained via monotone upstream-centered schemes for conservation laws (MUSCL) extrapolation coupled with a minmod limiter. Viscous fluxes are computed to second-order accuracy using central differencing. Using DPLR on an appropriate mesh (representing discretization of the flow domain) results in a volume solution containing the flow densities (of individual component species), Cartesian velocities, and energies (total and/or vibrational). Although DPLR has additional postprocessing capabilities to extract quantities of interest such as heat flux, skin friction, etc., it does not have built-in capabilities to extract boundary-layer quantities of interest such as the displacement and momentum thicknesses. These boundary-layer quantities have to be extracted from the computed solution through the use of specialized software.

The usual way of detecting the edge of a shear layer bounded to a nonadiabatic wall is to determine the point (along a line drawn normal to the wall) at which the total enthalpy of the flow reaches 99.5% of its freestream value. In the present work, however, a different approach was taken in determining the thermal/enthalpy edge of the wall-bounded shear layer. The method is intended to cope with possible overshoots or undershoots in computed enthalpy-ratio profiles. It is currently coded as a NASA Ames computer program named BLAYER, validated against the data of van Driest [7], and undergoing internal review before publication. Briefly, for each radial grid line off the wall, the method in BLAYER computes the curvature of the profile of total enthalpy ratio vs normalized wall distance. The location of the first significant curvature peak near the wall along this profile is taken as defining the edge of the boundary layer. More precisely, because curvature is not independent of data scaling, this peak curvature location is used to define a window containing the edge (and avoiding the shock region). The traditional edge method is then applied to determine when the profile first reaches 99.5% *of the peak enthalpy ratio within that window* (not necessarily one). This interpolated wall distance is the calculated boundary-layer thickness. The method matches the traditional method if the profile is well-behaved, but it handles anomalous profiles more robustly.

Although present in ballistic-range experiments of ablating materials such as graphite, laminar ablation mass-transfer (blowing) rates B' were not explicitly included in these viscous calculations or addressed explicitly in the resultant data correlations. Calculations based on the methodology reported in [8] showed that under past [1] and present ballistic-range test conditions, B' values for laminar ablation of graphite in air always corresponded to the oxidation regime (plateau) and were thus constant at the nominal low value of 0.17.

As can be seen in Fig. 1, the slope of the correlation fit in log–log coordinates is −45 deg; that is, the disturbance and transition parameters are inversely proportional to the first power. The resultant

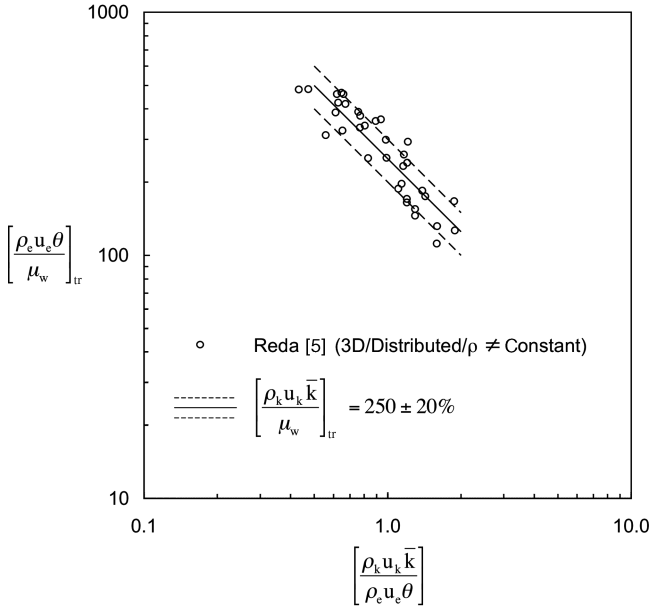

Fig. 1 Graphite nosetip transition data from ballistic-range experiments, analyzed using real-gas Navier–Stokes code; three-dimensional distributed roughness, compressible flows.

roughness-dominated transition model is thus equivalent to the statement that the critical-roughness Reynolds number for three-dimensional distributed roughness on blunt bodies in hypersonic flow is a constant: $[\rho_k u_k \bar{k}/\mu_w]_{tr} = 250 \pm 20\%$. The ±20% band about the mean correlation fit was chosen based on its inclusion of essentially all data points and, as such, it is a measure of both the repeatability of the experimental approach and the uncertainty of the correlation for actual design applications.

The regime defined by the existing database is $0.5 \leq [\rho_k u_k \bar{k}/\rho_e u_e \theta] \leq 2.0$, covering a factor of 4 in the disturbance parameter. To be of utility in any TPS design code, the lower and upper limits (asymptotes) must also be defined.

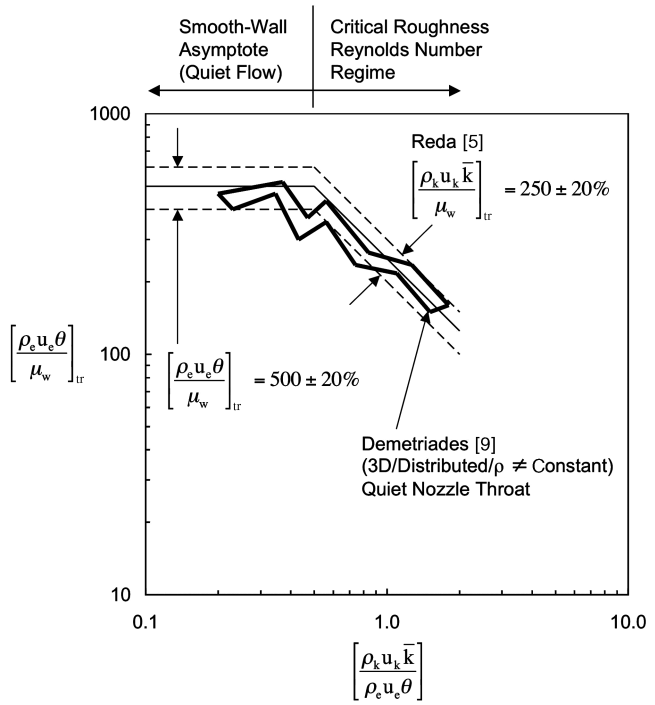

Fig. 2 Graphite nosetip transition data band from ballistic-range experiments compared with data of Demetriades [9] for three-dimensional distributed roughness in a quiet nozzle throat.

III. Extension to the Smooth-Wall Limit for Quiet Compressible Flows

Demetriades [9], explored the effects of three-dimensional distributed roughness (created with wire-mesh overlays of parametrically varied wire diameter) on transition in the nozzle throat of a quiet supersonic wind tunnel. He found corroborating evidence to support the ballistic-range results [4,5]: namely, a constant critical-roughness Reynolds number for transition of order 250 in the roughness-dominated regime (see Fig. 2). Note that a sonic-nozzle-throat flowfield closely simulates the flowfield over a blunt body in hypersonic flow, expanding over a concave surface from the stagnation conditions through Mach 1 to low supersonic Mach numbers.

In addition to this most important finding, Demetriades [9] was also able to define the smooth-wall asymptote for quiet flows,

$$\left[\frac{\rho_e u_e \theta}{\mu_w}\right]_{\text{tr,smooth}} = 500 \pm 20\%$$

by systematically reducing the roughness height scale to zero.

IV. Results of Recent Experiments

As noted in [1–5], the preablated graphite data shown in Fig. 1 were all measured during experiments conducted using range G at Arnold Engineering Development Center (AEDC) in the 1970s. The knowledge gained from this earlier research was transferred to the NASA Ames hypersonic ballistic range over the last few years and was used to conduct several new aerothermodynamic experiments discussed herein. Testing methodologies were reviewed in [10] and were expanded upon in [11]. Results from these new experiments are given in the following two subsections and are tabulated in Tables 1 and 2.

A. Three-Dimensional Distributed Roughness on Hemispheres in Hypersonic Free Flight

Flight hemispherical geometries with ablative TPS materials are of interest to NASA as being representative of Apollo and crew exploration vehicle (CEV) heat-shield configurations.

Figure 3 shows a schematic and a photograph of the 1.50-in.-diam bore-rider model used in recent NASA Ames experiments. Note that all experiments were conducted in free-flight mode, because a rail system such as that employed in range G at AEDC is currently not available.

Consistent with the established testing methodology [1–4], POCO FM-1 graphite hemispheres were preablated under low-pressure, low-Reynolds-number, laminar-flow conditions in the NASA Ames arc-jet complex. One model was sectioned to measure its surface-roughness-element heights via microscopy and the remainder of the ablated hemispheres were transformed into ballistic-range models without touching the ablated test surfaces.

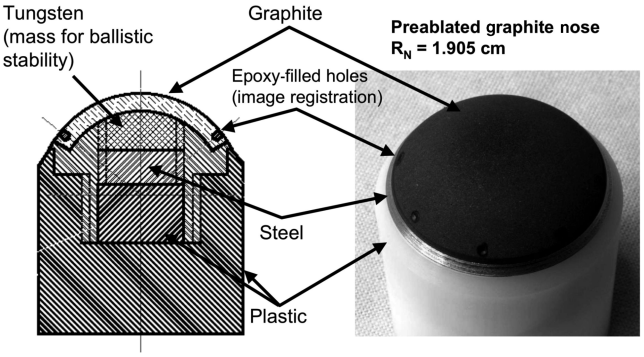

Fig. 3 Engineering drawing and photograph of preablated graphite hemispherical nosetip model.

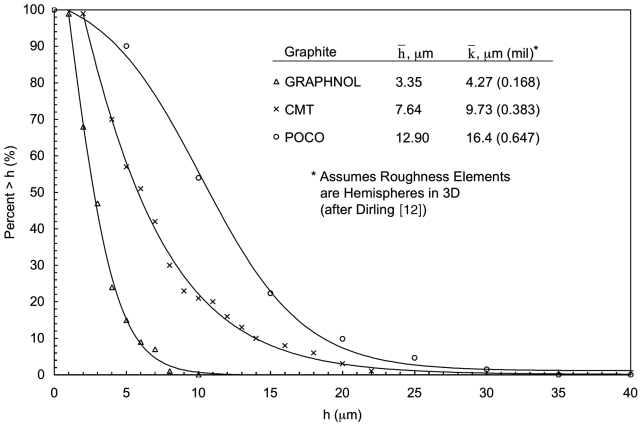

Fig. 4 Measured in-plane roughness-element-height distributions for three laminar-ablated graphites.

Figure 4 shows a comparison of measured in-plane roughness-element heights for laminar-ablated POCO graphite vs the two finer-grain graphites (Graphnol and CMT) used in earlier studies. A family of self-similar probability-of-exceedence distributions is evident. Average in-plane roughness-element heights $\bar{h}$ were transformed

Table 1 Tabulated results for preablated POCO graphite with a hemisphere geometry; $\bar{k} = 16.5$ μm (0.65 mil)

Shot	R_N, cm	P_∞,[a] atm	V_∞, km/s	T_{stag},[b] K	$(s/R_N)_{\text{tr}}$	X	Y_{tr}
2313	1.905	0.250	4.47	1417	0.1372	2.24	122.95
2326	1.905	0.250	4.44	1373	0.1099	2.25	97.72
2315	1.905	0.316	4.38	1601	0.1140	2.57	97.72
2312	1.905	0.375	4.33	1639	0.1210	2.81	107.63

[a]$T_\infty = 296$ K (air).
[b]As measured, equal to $T_{w,\text{tr}}$.

Table 2 Tabulated results for bead-blasted POCO graphite with a blunt-cone geometry; $\bar{k} = 14.5$ μm (0.57 mil)

Shot	R_N, cm	P_∞,[a] atm	V_∞, km/s	T_{stag},[b] K	$(s/R_N)_{\text{tr}}$	X	Y_{tr}	X
2332	0.9525	0.579	3.87	1570	0.2438	3.36	135.33	2.95[c]
2330	0.9525	0.657	3.77	1535	0.2757	3.51	156.66	3.09[c]
2337	0.9525	0.634	3.85	1666	0.1367	4.01	78.76	4.90[d]
2339	0.9525	0.706	3.71	1656	0.1660	4.15	92.76	5.08[d]
2329	0.9525	0.751	3.66	1679	0.1518	4.25	83.36	5.22[d]

[a]$T_\infty = 296$ K (air).
[b]As measured, equal to $T_{w,\text{tr}}$.
[c]For $\bar{k} = 12.5$ μm (0.49 mil).
[d]For $\bar{k} = 18.3$ μm (0.72 mil).

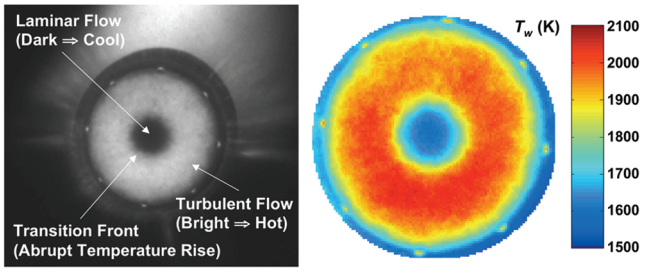

Fig. 5 Preablated hemispherical POCO graphite nosetip: a) ICCD camera image and b) global surface temperature distribution; $R_N = 1.905$ cm, $V_\infty = 4.5$ km/s, and $P_\infty = 0.317$ atm.

into three-dimensional peak-to-valley roughness-element heights $\bar{k}$ using the transformation proposed by Dirling [12] for assumed hemispherically shaped elements: $\bar{h} \times (4/\pi) = \bar{k}$.

Figure 5 shows the end-on-view surface-intensity distribution of a preablated POCO graphite hemisphere recorded by an intensified charge-coupled device (ICCD) camera during a recent hypersonic free-flight experiment at NASA Ames. Because all such images are recorded while the model is enveloped by a localized inert-gas (helium) plume, gas-cap radiation is eliminated. Further, because graphite is a blackbody, a direct calibration between surface intensity and surface temperature can be obtained using a blackbody-calibration source viewed on an identical optical path.

The right side of Fig. 5 shows the resultant measured global surface temperature distribution. Transition to turbulence along any ray emanating from the stagnation point is defined by an abrupt positive change in slope of the temperature-vs-location curve. Average transition locations for each image were calculated from crosscuts of the temperature maps taken every 2 deg circumferentially around the model image, then mathematically averaged.

Figure 6 shows transition results measured during four flights of preablated POCO graphite hemispheres, in comparison with the published GNOL and CMT graphite results. Note that to be acceptable for data analyses and inclusion in the final correlation, maximum pitch and yaw angles for the free-flight models had to be

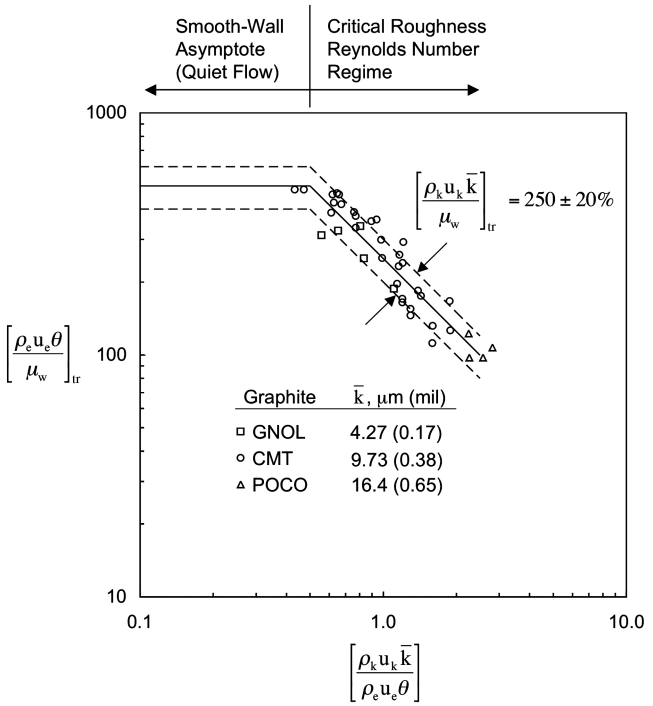

Fig. 6 Transition data for preablated graphite nosetips with three-dimensional distributed roughness; ballistic-range experiments analyzed using real-gas Navier–Stokes code.

measured at 5.0 deg or less throughout each free-flight trajectory. This requirement minimized the potential complexities of analyzing images that had suffered thermal smearing due to larger angle-of-attack oscillations.

POCO, being a rougher material, is characterized by higher values of the disturbance parameter (to order 2.5), and transition correspondingly occurs earlier, at lower transition Reynolds numbers (down to order 100).

What remained to be done at this point was to extend this transition correlation to still higher values of the disturbance parameter to determine whether a large-roughness/low-Reynolds-number asymptote could be defined. This is addressed in the next subsection.

B. Three-Dimensional Distributed Roughness on Blunt Large-Angle Cones in Hypersonic Free Flight

Blunt large-angle conical geometries with ablative TPS materials are of interest to NASA as being representative of Mars-entry and Titan-aerocapture heat-shield configurations.

Figure 7 shows an engineering schematic and a photograph of the bore-rider model chosen to represent this class of vehicles. POCO graphite was again selected as the test-surface material.

In this sequence of tests, facility scheduling and budget considerations led to a decision to preroughen these graphite test surfaces mechanically via bead-blasting, as opposed to using the established methodology of laminar ablation in an arc-jet facility. This approach, of necessity, inserts a human in the preroughening loop and thus requires that reproducibility be documented.

Figure 8 shows measured (via microscopy) in-plane roughness-element-height distributions for two separate attempts at bead-blasting POCO graphite discs using the same human-in-the-loop approach for each test. Reproducibility was found to be marginal. Using the combined data sets as a large-sample basis, test 1 showed a

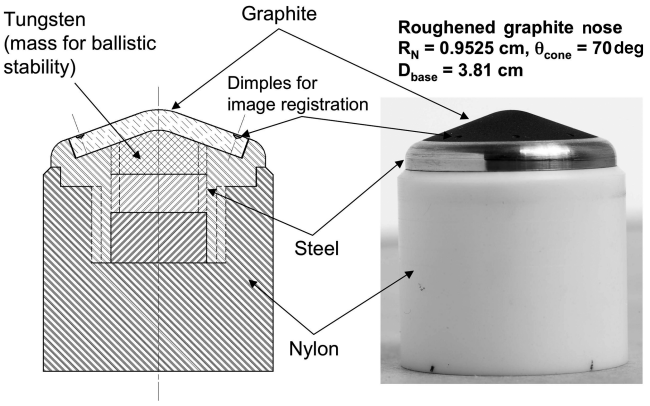

Fig. 7 Engineering drawing and photograph of bead-blasted POCO graphite model for blunt large-angle cone geometry.

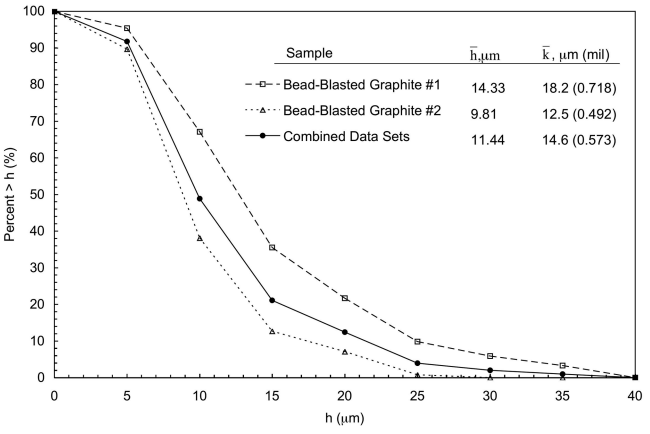

Fig. 8 Measured in-plane roughness-height distribution for two bead-blasted POCO graphite samples.

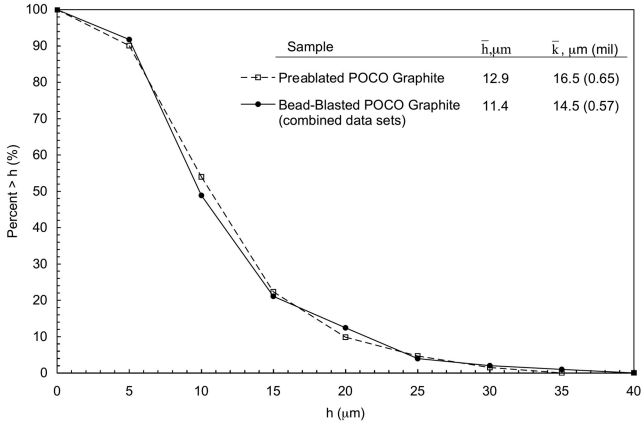

Fig. 9 Measured in-plane roughness-height distribution for POCO graphite preablated-vs-combined bead-blasted sets.

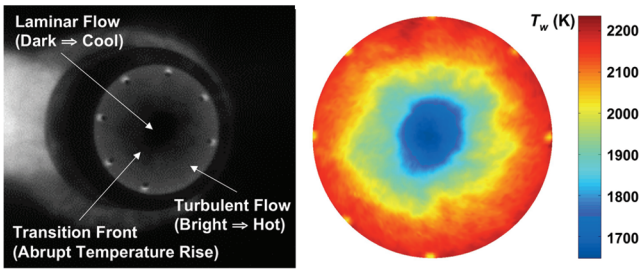

a) **b)**

Fig. 10 Bead-blasted blunt large-angle cone model: a) ICCD camera image and b) global surface temperature distribution; $R_N = 0.9525$ cm, $V_\infty = 4.5$ km/s, and $P_\infty = 0.75$ atm.

mean roughness height that was 25% above the combined-data-set value, whereas results of test 2 showed a mean roughness height that was 15% below the combined-data-set value. Recall that the uncertainty band on the partially completed transition correlation of Fig. 6 is ±20%, comparable with this mechanically imposed roughness uncertainty band.

Figure 9 shows a comparison of the combined data set for mechanical roughening vs the laminar-ablated-roughness distribution for the same material. Apparently, if one bead blasts the surface long enough, the mechanically imposed surface roughness pattern approaches the laminar-ablation-induced surface roughness pattern.

Figure 10 shows a two-part figure for blunt large-angle cone models that is comparable with that presented for hemispheres in Fig. 5. The as-recorded surface-intensity distribution is shown on the left, and the corresponding measured global surface temperature distribution is shown on the right. As before, the average transition-front location was defined by the locus of abrupt-slope-change locations measured along individual rays taken every 2 deg around the image. Likewise, as with all previous data-analysis efforts, real-gas Navier–Stokes calculations of model flowfields, including laminar boundary-layer development in these flowfields, were used to transform the experimental observations into the dimensionless parameters used to correlate transition results [6]. Only those flights that resulted in measured maximum pitch/yaw angles less than 5.0 deg over the complete trajectory were included in these final data analyses. These five images were recorded at range static pressures greater than or equal to 0.579 atm, and under such conditions, the mean transition front was always observed to occur on the blunt-nose portion of the model.

Figure 11 shows a composite plot of all measured transition results for both hemisphere and blunt large-angle cone geometries. Two observations were made: First, when using the combined-data-set average roughness value of 14.6 μm for mechanical roughening, all five of the blunt large-cone-angle data points correspond to a disturbance parameter of order 4, but clearly show significant variations in the transition Reynolds number parameter, ranging

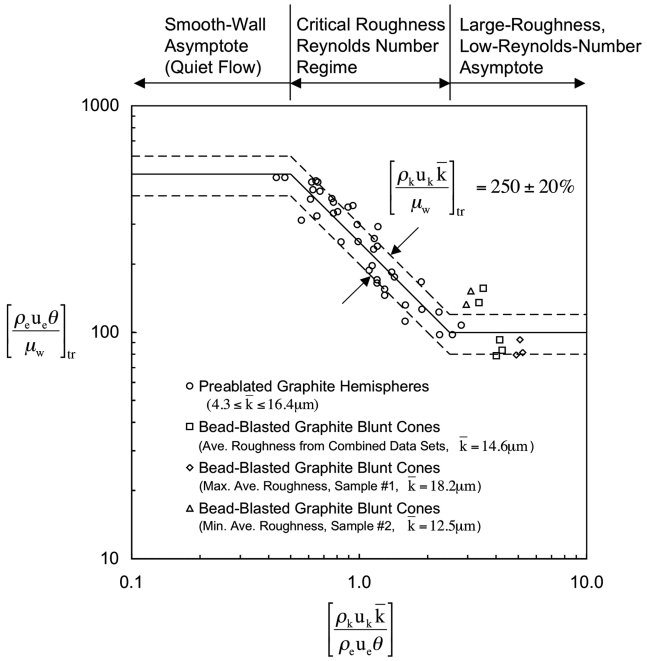

Fig. 11 Transition correlation for blunt bodies with distributed roughness in hypersonic free flight.

from order 80 to order 120. Such variations are consistent with the reproducibility uncertainties noted for the mechanical preroughening approach.

Expanding on this observation, if one assumes that the earlier transition data (the lowest Re_{tr} results) should be analyzed using the largest bead-blasting roughness height of 18.2 μm, and if one assumes that the later transition data (the highest Re_{tr} results) should be analyzed using the smallest bead-blasting roughness height of 12.5 μm, then these five data points separate into two clusters: one near a disturbance parameter of 3 and the other near a disturbance parameter of 5. The uncertainty band on mechanically induced surface roughness (+25 to −15%) thus yields uncertainties in the transition response that are consistent with the ±20% band noted in the present correlation.

From an overall perspective, the nozzle-throat data of Demetriades [9], the earlier graphite hemisphere data of Reda [1–5], and the new results presented herein, when combined, provide the TPS designer with a transition correlation covering all three regimes potentially encountered by an ablating blunt-body heat shield in atmospheric entry. The smooth-wall asymptote for the quiet-flow regime is

$$\left[\frac{\rho_k u_k \bar{k}}{\rho_e u_e \theta}\right] \le 0.5, \qquad \left[\frac{\rho_e u_e \theta}{\mu_w}\right]_{tr} = 500$$

The critical-roughness Reynolds number regime is

$$0.5 \le \left[\frac{\rho_k u_k \bar{k}}{\rho_e u_e \theta}\right] \le 2.5, \qquad \left[\frac{\rho_k u_k \bar{k}}{\mu_w}\right]_{tr} = 250$$

The large-roughness/low-Reynolds-number asymptote regime is

$$\left[\frac{\rho_k u_k \bar{k}}{\rho_e u_e \theta}\right] \ge 2.5, \qquad \left[\frac{\rho_e u_e \theta}{\mu_w}\right]_{tr} = 100$$

Within each transition regime, an uncertainty band of ±20% on the transition parameter is shown to be applicable.

In summary, the transition correlation presented in Fig. 11 is based on combined data sets wherein the surface mass flux was either zero [9] or a very low value, defined by the oxidation plateau for ablating graphite [8]. Further, the three-dimensional distributed-surface-roughness distribution in each case could be characterized by a single height scale: either the mesh-wire diameter or the average peak-to-valley height of a sand-grain-like roughness pattern.

More complex TPS materials (e.g., woven or fibrous materials such as carbon/carbon composites) are more difficult to characterize by a single/average height scale. Such materials could potentially be characterized by a single height scale by measuring the largest distributed roughness elements that form under laminar ablation (e.g., the step heights that form between axial and transverse fiber bundles). Transformation of such a physically measured height scale to its equivalent sand-grain roughness height for tripping would still need to be determined empirically using the test methodology first reported in [4].

Further, higher surface-mass-transfer rates (e.g., as encountered in the sublimation-vs-oxidation regimes for carbonaceous ablators) could also potentially modify the transition correlation of Fig. 11. Clearly, additional research is required.

V. Conclusions

Results of present ballistic-range transition experiments, when combined with published ballistic-range and quiet-wind-tunnel transition data, form the basis of a three-regime transition correlation applicable to the design of ablating blunt-body heat shields undergoing atmospheric entry.

Acknowledgements

A portion of the funding for this work was provided by the In-Space Propulsion program under task agreement M-ISP-03-18 to NASA Ames Research Center. David Bogdanoff and Dinesh Prabhu were supported by contract NNA04BC25C from NASA Ames Research Center to the Eloret Corporation.

References

[1] Reda, D. C., "Correlation of Nosetip Boundary-Layer Transition Data Measured in Ballistics-Range Experiments," Sandia National Labs., TR SAND79-0649, Nov. 1979.

[2] Reda, D. C., and Raper, R. M., "Measurements of Transition-Front Asymmetries on Ablating Graphite Nosetips in Hypersonic Flight," *AIAA Journal*, Vol. 17, No. 11, Nov. 1979, pp. 1201–1207.

[3] Reda, D. C., "Comparative Transition Performance of Several Nosetip Materials as Defined by Ballistics-Range Testing," *ISA Transactions*, Vol. 19, No. 1, 1980, pp. 83–98.

[4] Reda, D. C., "Correlation of Nosetip Boundary-Layer Transition Data Measured in Ballistics-Range Experiments," *AIAA Journal*, Vol. 19, No. 3, Mar. 1981, pp. 329–339.

[5] Reda, D. C., "Review and Synthesis of Roughness-Dominated Transition Correlations for Reentry Applications," *Journal of Spacecraft and Rockets*, Vol. 39, No. 2, Mar.–Apr. 2002, pp. 161–167.

[6] Wright, M. J., Candler, G. V., and Bose, D., "Data-Parallel Line Relaxation Method for the Navier–Stokes Equations," *AIAA Journal*, Vol. 36, No. 9, 1998, pp. 1603–1609.

[7] Van Driest, E. R., "The Problem of Aerodynamic Heating," *Aeronautical Engineering Review*, Vol. 15, No. 10, 1956, pp. 26–41.

[8] Chen, Y.-K., Milos, F. S., Reda, D. C., and Stewart, D. A., "Graphite Ablation and Thermal Response Simulation Under Arc-Jet Flow Conditions," 36th Thermophysics Conference, Orlando, FL, AIAA Paper 2003-4042, 23–26 June 2003.

[9] Demetriades, A., "Roughness Effects on Boundary-Layer Transition in a Nozzle Throat," *AIAA Journal*, Vol. 19, No. 3, 1981, pp. 282–289.

[10] Reda, D. C., Wilder, M. C., Bogdanoff, D. W., and Olejniczak, J., "Aerothermodynamic Testing of Ablative Reentry Vehicle Nosetip Materials in Hypersonic Ballistic-Range Environments," 1st U.S. Air Force Developmental Test & Evaluation Summit, Woodland Hills, CA, AIAA Paper 2004-6829, 16–18 Nov. 2004.

[11] Wilder, M. C., Reda, D. C., Bogdanoff, D. W., and Prabhu, D. K., "Free-Flight Measurements of Convective Heat Transfer in Hypersonic Ballistic-Range Environments," 39th AIAA Thermophysics Conference, Miami, FL, AIAA Paper 2007-4404, 25–28 June 2007.

[12] Dirling, R. B., Jr., "On the Relation Between Material Variability and Surface Roughness," 18th Structures, Structural Dynamics and Materials Conference, San Diego, CA, AIAA Paper 77-402, Mar. 1977.

R. Kimmel
Associate Editor